

Supporting Information for

Efficient Removal of Aqueous Cr(VI) Using Sulfur-Modified Biochar Derived from Anaerobic Digestate: Synergistic Mechanism for Reduction and Sorption

Kunlun Yang ^{a, b, c}, Yimei Wang ^a, Dengyang Wang ^a, Zengshuai Zhang ^{a, b, c}, Peng Gu ^{a, b, c}, Xueli Ren ^{a, b, c}, Hengfeng Miao ^{a, b, c, *},

a. School of Environment and Ecology, Jiangnan University, Wuxi 214122, PR China

b. Jiangsu Key Laboratory of Anaerobic Biotechnology, Jiangnan University, Wuxi 214122, PR China

c. Jiangsu Engineering Laboratory of Biomass Energy and Carbon Reduction Technology, Jiangnan University, Wuxi 214122, PR China

*Corresponding author: Hengfeng Miao, Jiangnan University, Wuxi 214122, China.

E-mail address: hfmiao@jiangnan.edu.cn

Table of Contents

Text S1 Purity of used chemical reagents

Text S2 Preparation of four types of digestate from anaerobic digestion of kitchen waste

Text S3 Data analysis

Text S4 Procedure for electrochemical experiments

Text S5 Coagulation settling effect of biogas slurry under different dosage of PFS

Text S6 The efficacy of Cr(III) removal from aqueous solutions under different initial pH

Text S7 Reuse test procedure

Fig. S1 SEM images and the corresponding EDS elemental mappings (C, O, S, Cl, K, Ca and Fe) of 900-2S@DBC

Fig. S2 SEM images and the corresponding EDS elemental mappings (C, O, S, Cl, K, Ca and Fe) of 900-0S@DBC

Fig. S3 SEM-EDS elemental analysis (C, O, S, Cl, K, Ca, Fe) of (a) 900-2S@DBC and (b) 900-0S@DBC

Fig. S4 N₂ Adsorption-Desorption Isotherm of (a) 900-2S@DBC, (b) 900-0S@DBC, (c) 900-1S@DBC, (d) 900-4S@DBC and (e) 800-2S@DBC

Fig. S5 Zero charge points of (a) 900-0S@DBC, (b) 900-1S@DBC, (c) 900-4S@DBC and (d) 800-2S@DBC

Fig. S6 (a) The intermolecular diffusion model curve and (b) adsorption kinetic curve of digestate biochar prepared under different PFS dosages. (c) The intermolecular diffusion model curve and (d) adsorption kinetic curve of digestate biochar prepared under different secondary pyrolysis temperature

Fig. S7 (a) Effect of 900-2S@DBC dosage on the reduction of Cr (VI); (b) The pH variation in the solution following reaction with varying dosages of 900-2S@DBC; (c) The concentration of Cr(VI) and Cr(III) in the solution after reaction under various initial pH conditions; (d) The concentration of Cr(VI) and Cr(III) in the solution were determined after reaction with varying dosages of 900-2S@DBC

Fig. S8 Effect of coexisting ions on Cr(VI) reduction (Experiment conditions: initial Cr(VI) = 10 mg/L, biochar dosage = 0.5 g/L, pH = 3.0 ± 0.3, T = 25 °C)

Fig. S9 Solution pH after the coexisting ion experiment

Fig. S10 XPS full spectrum of different materials

Table S1 Parameters of internal diffusion models for various types of digestate biochar

Table S2 Parameters of adsorption kinetics curves for various types of digestate biochar

Table S3 Summary of removal effects of Cr(VI) in other materials

Text S1 Purity of used chemical reagents

The purity of polyferric sulfate (PFS) is Fe content of 21 %. Polyacrylamide (PAM) is excellent grade pure and non-ionic. Potassium dichromate ($K_2Cr_2O_7$), hydrochloric acid (HCl), sodium hydroxide (NaOH), phosphoric acid (H_3PO_4), sulfuric acid (H_2SO_4), potassium bromate ($KBrO_3$) and furfuryl alcohol are analytically pure. Benzoquinone (BQ) is excellent grade pure.

Text S2 Preparation of four types of digestate from anaerobic digestion of kitchen waste

The initial slurry of kitchen waste should be placed in a 37 °C, 120 r/min oscillator for continuous fermentation over a period of 7 days, ensuring an anaerobic environment throughout the process and maintaining the pH of the kitchen waste slurry at 10. Ca(OH)₂ and partial KOH were used for adjusting the pH. Following fermentation, the fermentation broth undergoes coagulation and precipitation to facilitate the separation of biogas slurry from the sludge. The specific operational procedures for coagulation and sedimentation are as follows: sequentially add 0 mg/L, 100 mg/L, 200 mg/L, and 400 mg/L of PFS to the kitchen waste slurry; adjust the stirring speed to 350 r/min and vigorously stir for 1 minute; subsequently introduce an additional dosage of 15 mg/L of PAM, maintain the stirring speed at 350 r/min, and continue vigorous stirring for another minute; then reduce the stirring speed to 100 r/min and stir gently for a duration of 15 minutes; finally allow settling for a period of 30 minutes followed by separation of supernatant from digestate. After undergoing solid-liquid separation, the digestate is initially subjected to a drying process in an oven set at 105 °C for a duration of 24 hours. Then, it is finely ground and subsequently passed through a 60-mesh sieve for further refinement. The resulting digestate is then meticulously recorded as 0-DS, 1-DS, 2-DS, and 4-DS correspondingly.

Text S3 Data analysis

The biochar adsorption for Cr(VI) was quantified using Equation (1) in order to comprehensively assess its removal capacity.

$$q_e = \frac{(C_0 - C_e)V}{m} \quad (1)$$

Where q_e (mg/g) is the equilibrium adsorption amount of Cr(VI); C_0 (mg/L) is the initial concentration of Cr(VI), and C_e (mg/L) is the equilibrium concentration of Cr(VI); V (mL) is the volume of solution; and m (mg) is the adsorbent dosage.

The removal rate of Cr(VI) can be determined by employing Equation (2).

$$\eta = \frac{C_0 - C_e}{C_0} \times 100\% \quad (2)$$

To further investigate the chromium removal capacity of biochar, we employed quasi-first-order and quasi-second-order models to analyze the kinetics of Cr(VI) and Cr(III) removal. The quasi-first-order kinetic model and quasi-second-order kinetic model can be used to further analyze the adsorption process of Cr(VI) and Cr(III), and the equations of the quasi-first-order kinetic model (Eqs. (3)) and quasi-second-order kinetic model (Eqs. (4)) are as follows:

$$\ln(q_e - q_t) = \ln q_e - k_1 t \quad (3)$$

where q_e and q_t (mg g⁻¹) represent the adsorption capacity at equilibrium and the adsorption capacity at time t , respectively; and k_1 (min⁻¹) represents the reaction rate constant for the quasi-first-order kinetic model.

$$\frac{t}{q_t} = \frac{1}{k_2 q_e^2} + \frac{t}{q_e} \quad (4)$$

where k_2 (g mg⁻¹ min⁻¹) represents the reaction rate constant for the quasi second-

order kinetic model.

The intraparticle diffusion model was employed to investigate the adsorption kinetics of the adsorbents, and the obtained data were fitted and analyzed using Equation (5):

$$Q_t = t^{0.5} \times K_p + C \quad (5)$$

where K_p is the intraparticle diffusion rate constant ($\text{mg} \cdot \text{min}^{-0.5} \cdot \text{g}^{-1}$) and C is the internal diffusion modeling constant.

Text S4 Procedure for electrochemical experiments

Electrochemical experiments were carried out on the prepared materials by using a typical three-electrode system on an electrochemical workstation. The Ag/AgCl electrode and Pt wire were used as reference electrode and counter electrode, respectively, and the catalyst coated on the surface was used as the working electrode. The preparation method of the working electrode is as follows: Firstly, the fluorine-containing tin oxide (FTO) conductive glass is washed and dried, and 10 mg catalyst is added to 1 ml ethanol. After shaking, 10 μL Nafion reagent (5%) is slowly dropped, and the material is ultrasonically dispersed for 30 min. 0.1 mL of the mixed solution containing the sample was dropped on the conductive glass (1.5 cm \times 1.5 cm), vacuum dried and repeated many times until the material was evenly covered with the whole glass, and the working electrode was obtained by drying overnight at room temperature. EIS measurements were performed in the range of -0.2~1.8 V, with a rate of 20 mV \cdot s $^{-1}$ and 5 mM Na₂SO₄ aqueous solution as the electrolyte.

Text S5 Coagulation settling effect of biogas slurry under different dosage of PFS

The coagulation experiment of biogas slurry revealed settling times of 104 minutes for 900-0S@DBC, 47 minutes for 900-1S@DBC, 37 minutes for 900-2S@DBC, and 38 minutes for 900-4S@DBC. Correspondingly, the removal rates of COD were found to be 12%, 17%, 28% and 21% respectively. The optimal coagulant dosage for achieving the best sedimentation effect under these conditions could be concluded to be 200mg/L of PFS.

Text S6 The efficacy of Cr(III) removal from aqueous solutions under different initial pH

Revealing a decline in the concentration of Cr(III) with increasing pH was observed. When the pH was 2, the adsorption capacity of 900-2S@DBC for Cr(III) was relatively low; however, at a pH of 3, it exhibited a significantly enhanced removal efficiency for Cr(III). The pH of 2 was found to promote the reduction of Cr(VI) while not favoring the chelation of Cr(III). On the other hand, an initial pH of 3 exhibited a significant removal effect on Cr(III) due to the ability of 900-2S@DBC to elevate the solution's pH after reaction, facilitating the removal process based on Cr(VI) reduction.

Text S7 Reuse test procedure

After the reaction equilibrium, the reactive saturated material was immersed in NaOH (0.1mol/L) solution and subjected to continuous magnetic agitation for 60min at 25°C to promote the desorption of pollutants. Ultra-pure water was capable of effectively removing desorbed chromium ions through continuous washing multiple times.

Fig. S1 SEM images and the corresponding EDS elemental mappings (C, O, S, Cl, K, Ca and Fe) of 900-2S@DBC

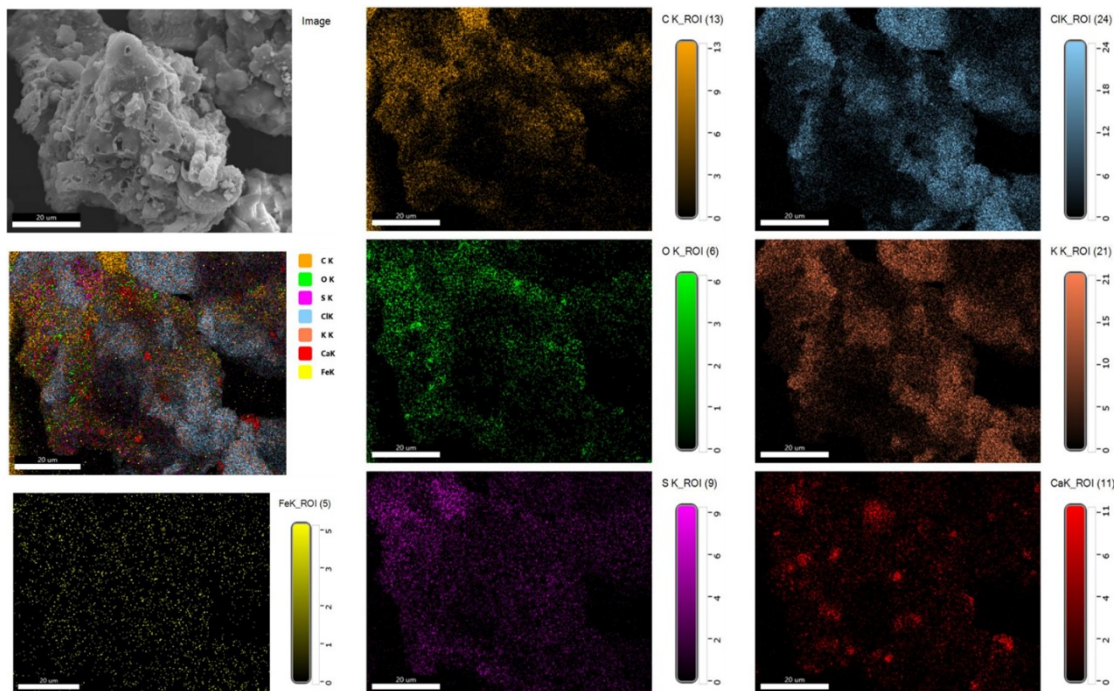


Fig. S2 SEM images and the corresponding EDS elemental mappings (C, O, S, Cl, K, Ca and Fe) of 900-0S@DBC

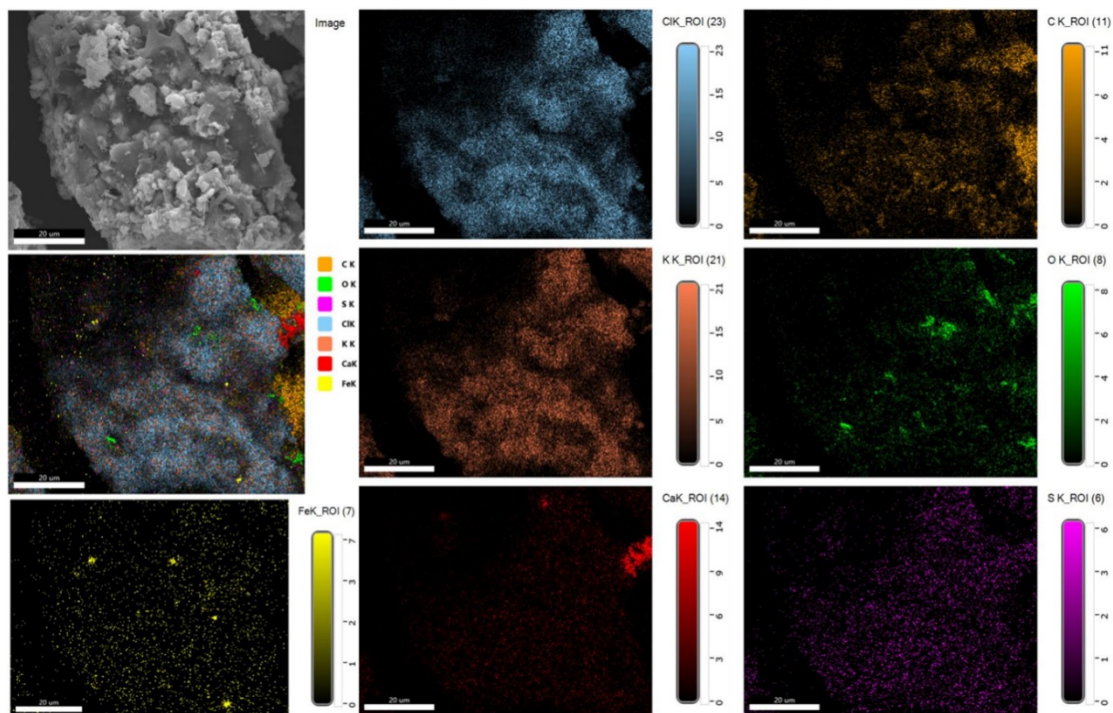
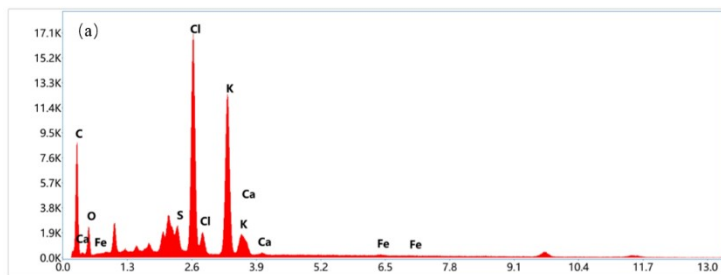
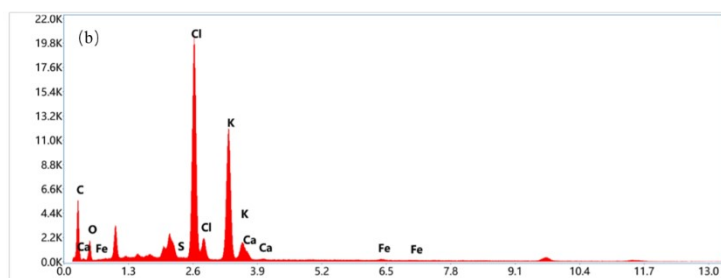


Fig. S3 SEM-EDS elemental analysis (C, O, S, Cl, K, Ca, Fe) of (a) 900-2S@DBC and (b) 900-0S@DBC



C K	66.0	81.6	223.2
O K	8.9	8.3	59.8
S K	2.4	1.1	218.7
Cl K	10.2	4.3	779.2
K K	10.9	4.1	628.8
Ca K	1.3	0.5	59.8
Fe K	0.2	0.1	5.1



C K ²	61.4 ²	79.0 ²	133.5 ²
O K ²	8.9 ²	8.6 ²	45.4 ²
S K ²	1.3 ²	0.6 ²	98.2 ²
Cl K ²	14.4 ²	6.3 ²	899.6 ²
K K ²	12.6 ²	5.0 ²	581.2 ²
Ca K ²	1.0 ²	0.4 ²	39.4 ²
Fe K ²	0.3 ²	0.1 ²	6.1 ²

Fig. S4 N₂ Adsorption-Desorption Isotherm of (a) 900-2S@DBC, (b) 900-0S@DBC, (c) 900-1S@DBC, (d) 900-4S@DBC and (e) 800-2S@DBC

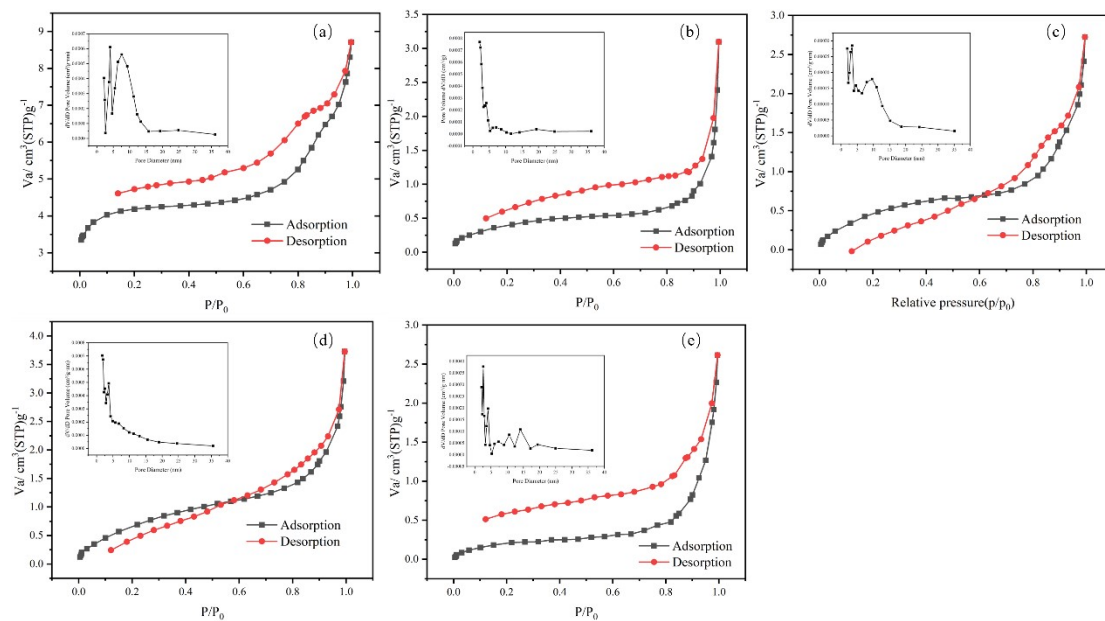


Fig. S5 Zero charge points of (a) 900-0S@DBC, (b) 900-1S@DBC, (c) 900-4S@DBC and (d) 800-2S@DBC

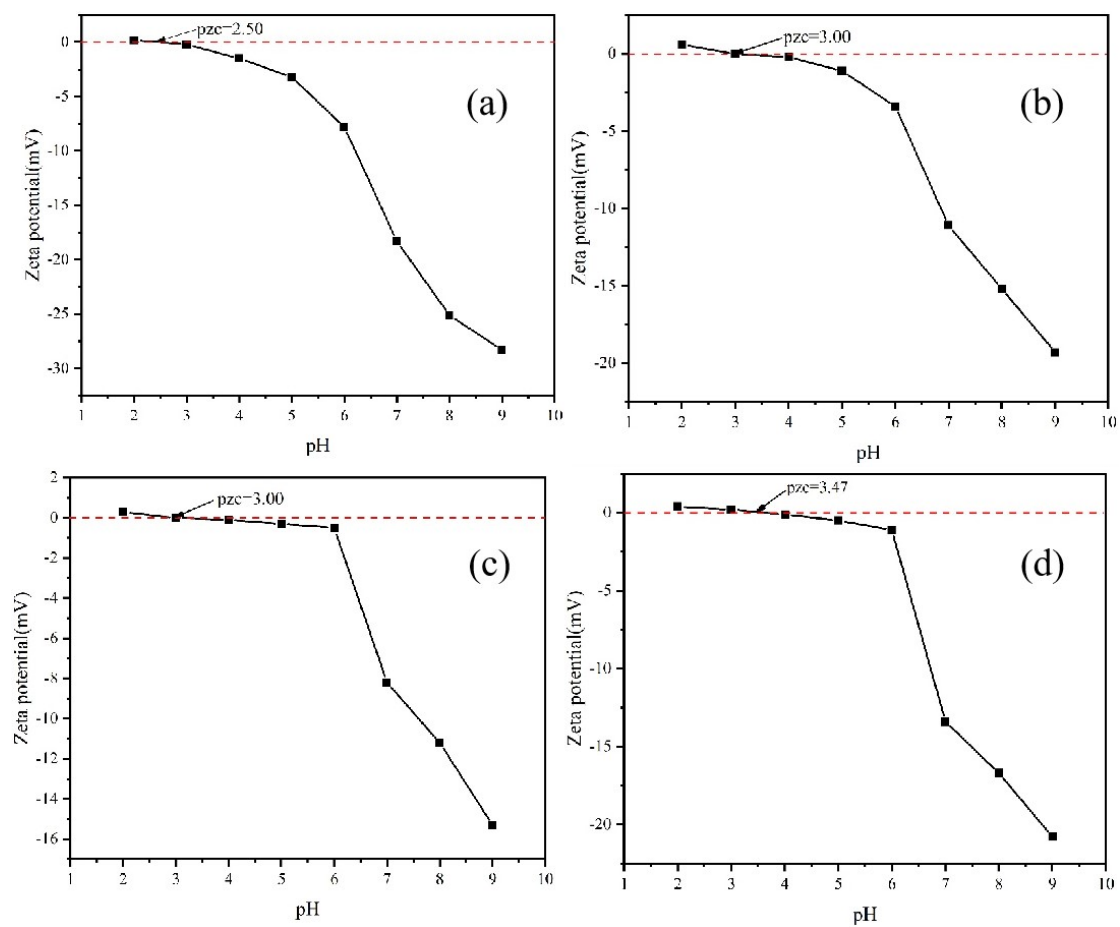


Fig. S6 (a) The intermolecular diffusion model curve and (b) adsorption kinetic curve of digestate biochar prepared under different PFS dosages. (c) The intermolecular diffusion model curve and (d) adsorption kinetic curve of digestate biochar prepared under different secondary pyrolysis temperature

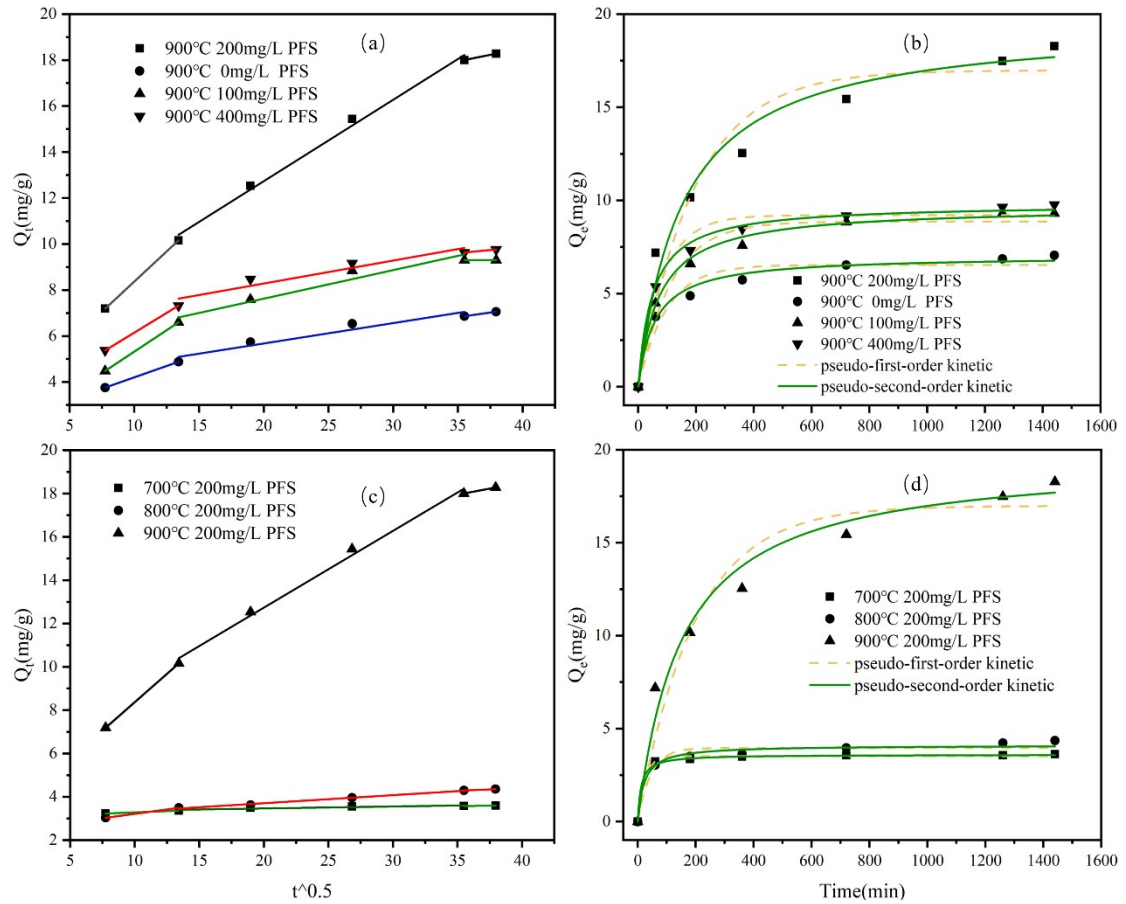


Fig. S7 (a) Effect of 900-2S@DBC dosage on the reduction of Cr (VI); (b) The pH variation in the solution following reaction with varying dosages of 900-2S@DBC; (c) The concentration of Cr(VI) and Cr(III) in the solution after reaction under various initial pH conditions; (d) The concentration of Cr(VI) and Cr(III) in the solution were determined after reaction with varying dosages of 900-2S@DBC

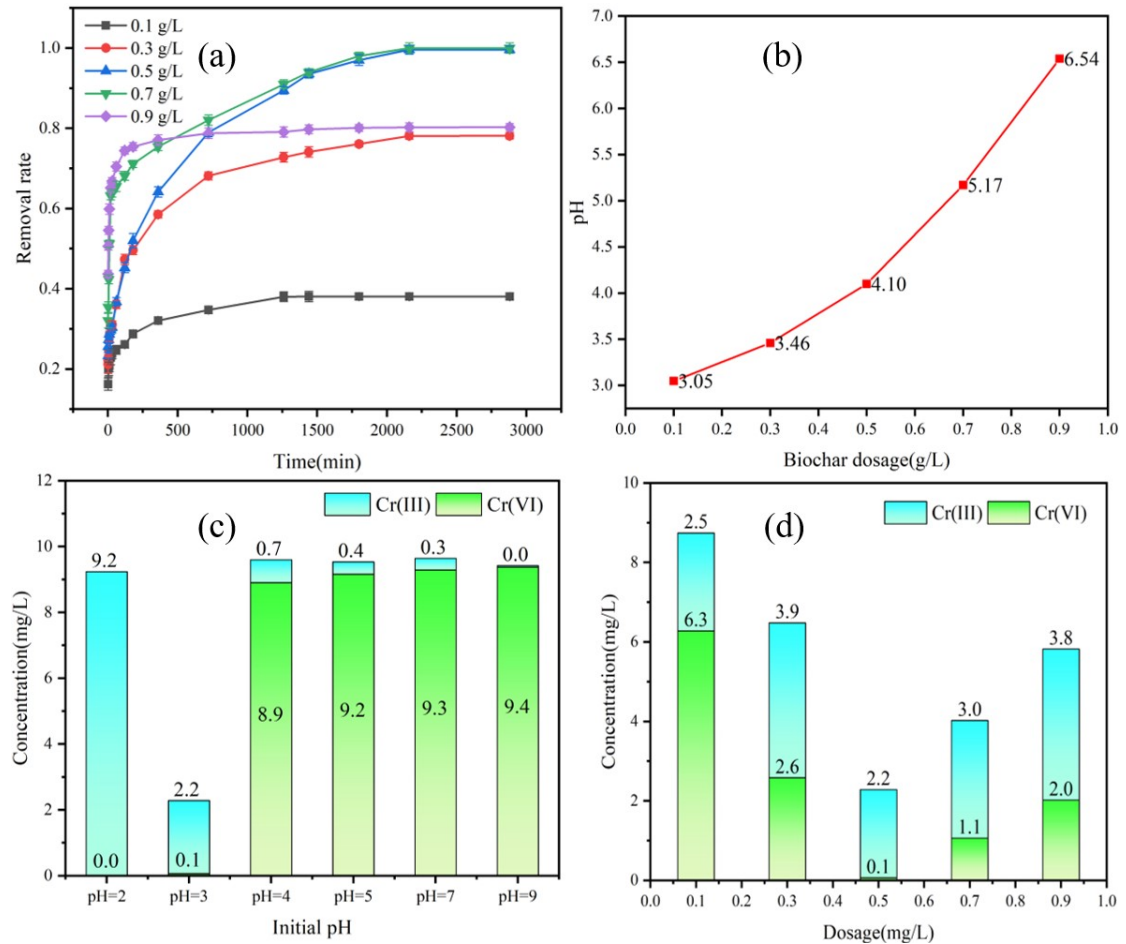


Fig. S8 Effect of coexisting ions on Cr(VI) reduction (Experiment conditions: initial Cr(VI) = 10 mg/L, biochar dosage = 0.5 g/L, pH = 3.0 ± 0.3, T = 25 °C)

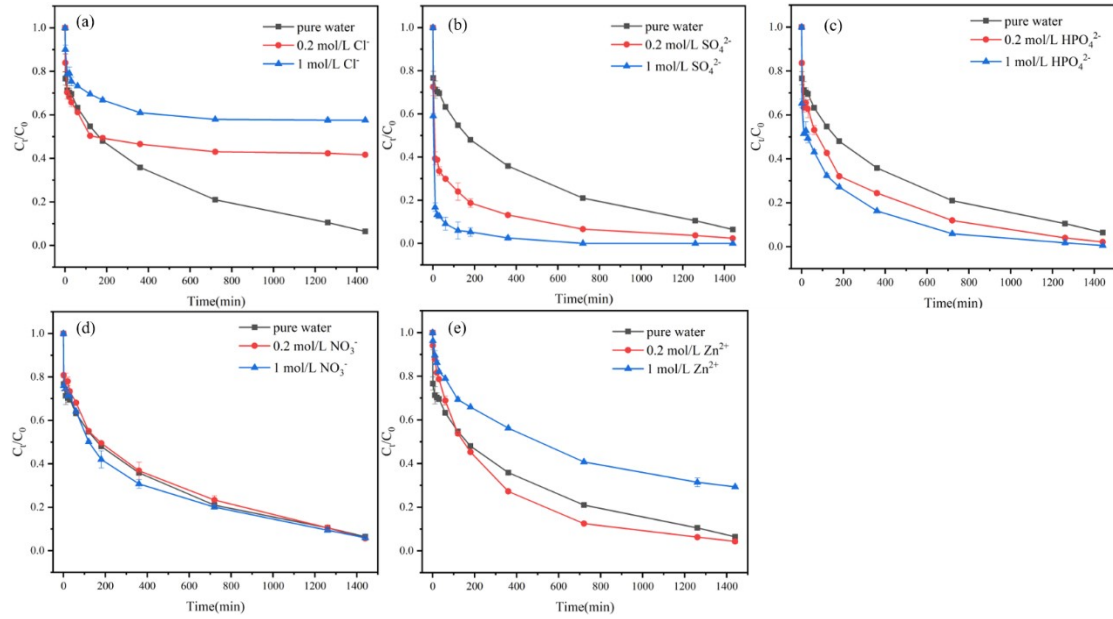


Fig. S9 Solution pH after the coexisting ion experiment

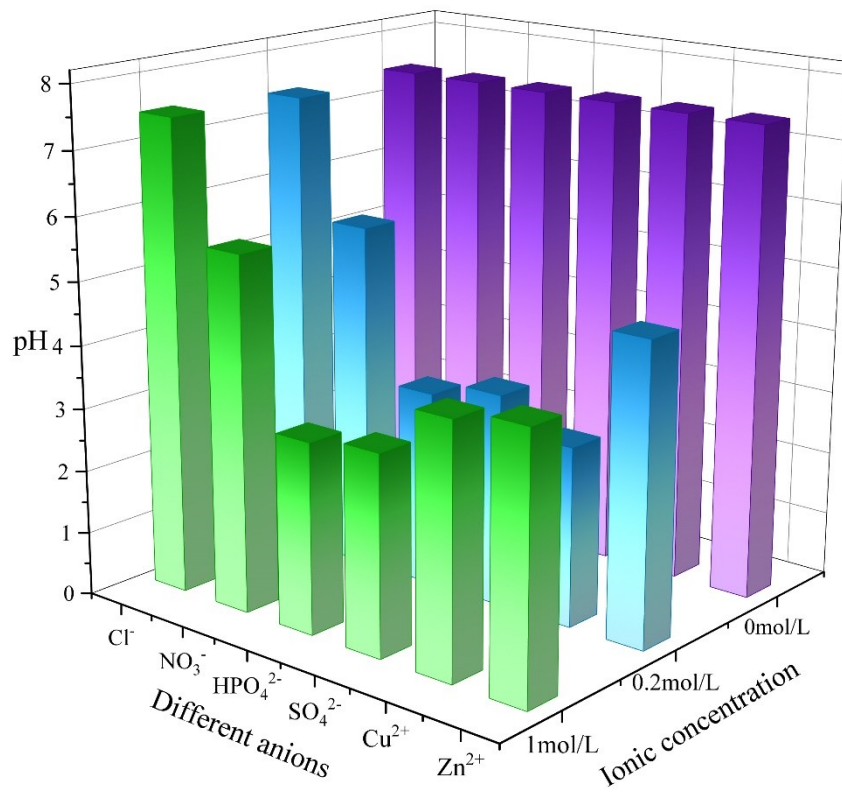


Fig. S10 XPS full spectrum of different materials

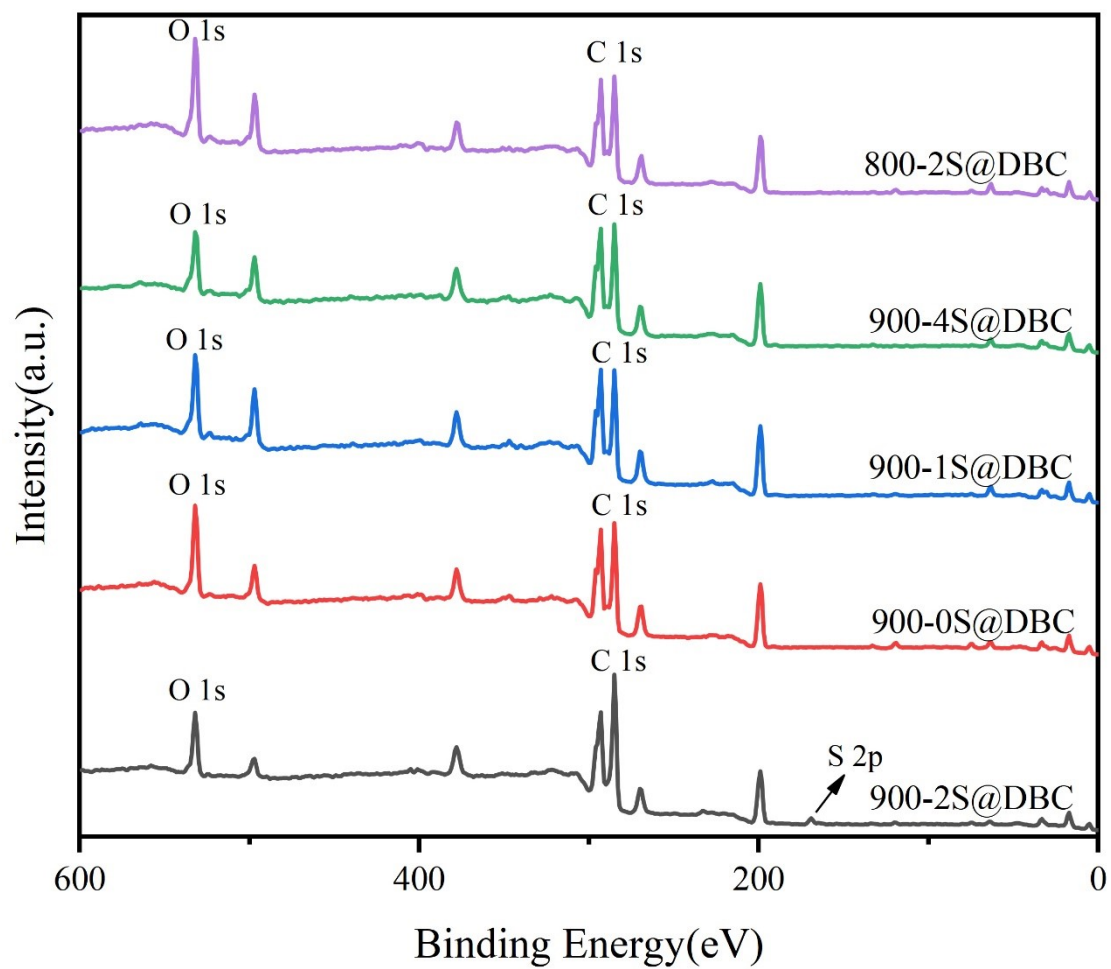


Table S1 Parameters of internal diffusion models for various types of digestate biochar

	K_{d1}	C_1	R^2	K_{d2}	C_2	R^2	K_{d3}	C_3	R^2
	mg/g	mg/g							
	$\cdot \text{min}^{1/2}$								
700- 2S@D BC	0.02 33	3.0540	1.000 0	0.009 1	3.2851	0.812 4	0.083 1	3.2862	1.000 0
800- 2S@D BC	0.08 15	2.4051	1.000 0	0.037 2	2.9662	0.992 2	0.023 0	3.4826	1.000 0
900- 2S@D BC	0.52 38	3.1372	1.000 0	0.354 3	5.6502	0.993 8	0.111 7	14.044 0	1.000 0
900- 0S@D BC	0.19 79	2.2295	1.000 0	0.088 7	3.9072	0.929 1	0.080 8	3.9967	1.000 0
900- 1S@D BC	0.37 25	1.6031	1.000 0	0.124 1	5.1461	0.945 1	0.021 5	9.3069	1.000 0
900- 4S@D BC	0.34 34	2.7196	1.000 0	0.099 9	2.8885	0.913 7	0.053 9	7.7250	1.000 0

Table S2 Parameters of adsorption kinetics curves for various types of digestate biochar

	Pseudo first order model			Pseudo second order model		
	Q_e	k_1	R^2	Q_e	k_2	R^2
700-2S@DBC	3.53	0.0414	0.925	3.60	0.25×10^{-5}	0.996
800-2S@DBC	3.96	0.0229	0.937	4.10	0.11×10^{-5}	0.963
900-2S@DBC	16.99	0.0051	0.946	19.57	0.34×10^{-5}	0.982
900-0S@DBC	6.54	0.0104	0.953	7.04	0.02×10^{-6}	0.960
900-1S@DBC	8.87	0.0088	0.965	9.66	0.01×10^{-6}	0.969
900-4S@DBC	9.21	0.0119	0.955	9.82	0.02×10^{-6}	0.973

Table S3 Summary of removal effects of Cr(VI) in other materials

Material name	Adsorption capacity (mg/g)	Reaction condition	Stability	Reference
N doping on sludge biochar (NSBC)	25.93	$C_0=100$ mg/L, pH=3, dosage=8 g/L	The removal efficiency of Cr (VI) by NSBC decreased from 92.31% to 76.62% after three repeated experiments	1
Fe-containing sludge biochar (FSBC)	24.33	$C_0=50$ mg/L, pH=3, dosage=2 g/L	None	2
Apple wood biochar (AW)	5.14	$C_0=50$ mg/L, pH=2, dosage=10 g/L	None	3
Magnetic biochar (MMABC)	25.27 mg/g	$C_0=10$ mg/L, pH=3, dosage=5 g/L	None	4
sulfate reducing sludge-based biochar(SBC-500)	5.84	$C_0=100$ mg/L, pH=4, dosage=1 g/L	The removal rate of SBC-500 was 91.98% after 5 cycles of adsorption-desorption98% °	5
Magnetic modified-corn cob biochar	25.94	$C_0=10$ mg/L, pH=3, dosage=0.4 g/L	None	6
hazelnut shell biochar	11.21	$C_0=50$ mg/L, pH=2, dosage=10 g/L	None	7
oak wood biochar (ZnO/BC)	4.99	$C_0=50$ mg/L, pH=2, dosage=10 g/L	None	8
ZnO nanoparticles on biochar derived from waste water hyacinth	24.0	$C_0=50$ mg/L, pH=2, dosage=10 g/L	The removal rate of 5 cycles was maintained at 67.1%	9

References

1. M. Ma, P. Wang and Z. Zhai, Effect of N doping on sludge biochar driving Cr(VI) removal from aqueous solution, *Desalination and Water Treatment*, 2024, 319: 100435.
2. W. Tang, H. Zhang and S. Huang, Removal Cr(VI) from tunneling wastewater by Fe-containing sludge biochar: The role of endogenous iron, *Desalination and Water Treatment*, 2024, 318: 100306.
3. N. Liu, Y. Zhang, C. Xu, P. Liu, J. Lv, Y. Liu and Q. Wang, Removal mechanisms of aqueous Cr(VI) using apple wood biochar: a spectroscopic study, *Journal of Hazardous Materials*, 2020, 384: 121371.
4. X. Zhang, L. Lv, Y. Qin, M. Xu, X. Jia and Z. Chen, Removal of aqueous Cr(VI) by a magnetic biochar derived from *Melia azedarach* wood, *Bioresource Technology*, 2018, 256: 1-10.
5. R. Ma, X. Yan, X. Pu, X. Fu, L. Bai, Y. Du, M. Cheng and J. Qian, An exploratory study on the aqueous Cr(VI) removal by the sulfate reducing sludge-based biochar, *Separation and Purification Technology*, 2021, 276: 119314.
6. H. Le Phuong, V. Huu Tap, N. Lan Huong, M. Duy-Hung, V. Thuy Trang, L. T. Ha and X. C. Nguyen, Removal of Cr(VI) from aqueous solution using magnetic modified biochar derived from raw corncob, *New Journal of Chemistry*, 2019, 43: 18663-18672.
7. Y. Zhang, Y. Tang, R. Yan, J. Li, C. Li and S. Liang, Removal performance and

- mechanisms of aqueous Cr (VI) by biochar derived from waste hazelnut shell, *Environmental Science and Pollution Research*, 2023, 30: 97310–97318.
8. N. Liu, Y. Zhang, P. Liu, J. Lv, Y. Liu, L. Ding and Y. Yang, Removal efficiency and mechanisms of dissolved Cr(VI) using oak wood biochar, *Desalination and Water Treatment*, 2019, 166: 334-343.
 9. J. Yu, C. Jiang, Q. Guan, P. Ning, J. Gu, Q. Chen, J. Zhang and R. Miao, Enhanced removal of Cr(VI) from aqueous solution by supported ZnO nanoparticles on biochar derived from waste water hyacinth, *Chemosphere*, 2018, 195: 632-640.